A&A 444, 305–317 (2005)
DOI: 10.1051/0004-6361:20053290

Astronomy & Astrophysics

Atomic data and spectral line intensities for Ca XIII⋆

E. Landi[1] and A. K. Bhatia[2]

[1] Artep, Inc, Ellicott City, MD 21042, USA and Naval Research Laboratory, Washington DC, 20375-5320, USA
e-mail: landi@poppeo.nrl.navy.mil
[2] NASA/Goddard Space Flight Center Greenbelt, Maryland 20771 USA

Received 22 April 2005 / Accepted 16 August 2005

ABSTRACT

Electron impact collision strengths, energy levels, oscillator strengths and spontaneous radiative decay rates are calculated for Ca XIII. The configurations used are $2s^22p^4$, $2s2p^5$, $2p^6$, $2s^22p^33s$, $2s^22p^33p$ and $2s^22p^33d$ giving rise to 86 fine-structure levels in intermediate coupling. Collision strengths are calculated at five incident energies (40, 80, 120, 160 and 200 Ry) in the distorted wave approximation. Excitation rate coefficients are calculated as a function of electron temperature by assuming a Maxwellian electron velocity distribution. Using the excitation rate coefficients and the radiative transition rates, statistical equilibrium equations for level populations are solved at electron densities covering the range of 10^8–10^{14} cm^{-3} at an electron temperature of $\log T_e(\mathrm{K}) = 6.5$, corresponding to maximum abundance of Ca XIII. Relative and absolute spectral line intensities are calculated, and their diagnostic relevance is discussed. This dataset will be made available in the next version of the CHIANTI database.

Key words. atomic data – Sun: corona – Sun: UV radiation

1. Introduction

Spectral lines emitted by calcium ions have routinely been identified in the spectra of solar plasmas under all conditions (Curdt et al. 2004), since the abundance of Ca relative to hydrogen is rather high, being 8.51×10^{-6}. At temperatures between 1 and 10 MK, typical of active regions and flares, calcium ions belonging to hydrogen to neon isoelectronic sequences can be easily observed. Among them, Ca^{+12} (Ca XIII) provides several lines that can be used for density and temperature diagnostics. Ca XIII belongs to the oxygen isoelectronic sequence, and emits lines in the visible and ultraviolet wavelength ranges from transitions within the ground configuration, or from allowed transitions within the $2s^22p^33l$ (l = s, p, d) configurations, in the EUV between 110 and 200 Å from allowed $2s^22p^4$–$2s2p^5$ transitions, and in the soft X-rays, from transitions between one $2s^22p^33l$ (l = s, p, d) level and one level in the $n = 2$ complex. Ca XIII lines have been observed in the solar spectrum (i.e. Jefferies et al. 1971; Acton et al. 1985; Feldman et al. 2000; Curdt et al. 2004), and have been used to study the physical properties of quiet Sun (Landi & Feldman 2003), active regions (i.e. Feldman et al. 2003) and flares (Feldman et al. 2004). Ca XIII lines have also been observed in the laboratory in many occasions, and those observations have led to the identification of all the levels in the $n = 2$ complex and several levels in the $2s^22p^33l$ (l = s, p, d) configurations (Bromage & Fawcett 1977; Doschek et al. 1973; Fawcett & Hayes 1975; Kaufman et al. 1982; Soukhanovskii et al. 2000).

Ca XIII lines can provide diagnostic pairs for the measurement of the electron density and temperature, and can also be used for emission measure, differential emission measure and velocity diagnostics; but in order to be used for these purposes, atomic data and transition rates are necessary to calculate line emissivities. However, Ca XIII has been neglected in the literature, so that intermediate coupling collision rates are available only for transitions within the 10 lowest levels, and for a few $2s^22p^33s$ lines (only in LS coupling); all other transitions have been neglected (despite their lines having been observed); moreover, the atomic models used for those calculations are rather limited, due to computer power limitations at the time when those calculations were performed.

Recently, Zhang & Sampson (2002) have calculated complete sets of atomic data and collision rates for the three lowest configurations of many ions in the O-like sequence, including Ca XIII. These calculations replace older collision strengths from Mason (1975), which also included only the lowest three configurations. However, the omission of the $2s^22p^23l$ configurations (l = s, p, d) in these calculations has two important consequences: these additional configurations can influence the wavefunctions of the lower configurations, so that transition rates calculated with models that omit the $n = 3$ configurations might be of limited accuracy, and their levels (additional 76 levels) can be important contributors to the level populations of the levels of the lower configurations via radiative

⋆ Full Table 2 is only available in electronic form at the CDS via anonymous ftp to cdsarc.u-strasbg.fr (130.79.128.5) or via http://cdsweb.u-strasbg.fr/cgi-bin/qcat?J/A+A/444/305

cascading. Also, these configurations generate spectral lines in the 30–50 Å and 600–800 Å spectral range that can be important for plasma diagnostics. Baliyan & Bhatia (1994) included these configurations in an R-Matrix calculation of collision rates, but they provided results in LS-Coupling, while intermediate coupling are needed for diagnostic purposes.

The aim of the present paper is to calculate a complete, self-consistent and accurate set of atomic data and transition rates for the $2s^2 2p^2 3l$ (l = s, p, d) configurations. We will make use of the University College London suite of codes to calculate a new, ab initio set of atomic energy levels, Einstein coefficients, oscillator strengths and collision strengths, necessary to calculate the synthetic spectrum of Ca XIII.

In Sect. 2 we describe the adopted model and the calculations, and in Sect. 3 we use the results to calculate level populations and line emissivities for Ca XIII. We compare our transition rates with those obtained from earlier work in Sect. 4. Predicted emissivities for the strongest transitions in the EUV range are compared with laboratory observations in Sect. 5. The diagnostic potential of Ca XIII lines is illustrated in Sect. 6. Section 7 summarizes the present work.

2. Atomic data

The atomic data have been calculated using computer programs originally developed at University College London. These programs have been updated over the years. The energy levels, oscillator strengths, and radiative transition rates have been calculated by using the Superstructure program described by Eissner et al. (1974). We have used two different models. In the first model, six configurations were included ($2s^2 2p^4$, $2s2p^5$, $2p^6$, $2s^2 2p^3\ 3l$, l = s, p, d), giving rise to 86 fine-structure levels. In the second model, a larger set including 24 configurations was adopted:

$2s^2 2p^4$
$2s2p^5$
$2p^6$

$2s^2 2p^3 3l$ l = s, p, d
$2s2p^4 3l$ l = s,p,d
$2p^5 3l$ l = s,p,d

$2s^2 2p^3 4l$ l = s, p, d, f
$2s2p^4 4l$ l = s, p, d, f
$2p^5 4l$ l = s, p, d, f.

The 24-configuration model was used in order to include all configurations in the complexes that included the six configurations for which we calculate collision excitation rates, plus other configurations that might provide significant contributions to the wave functions.

The wavefunctions are of configuration interaction type and each configuration is expanded in terms of Slater orbitals. The radial functions are calculated in a scaled Thomas-Fermi-Amaldi potential. The potential depends upon parameters λ_l which are determined variationally by optimizing the weighted sum of the term energies. For the 6-configuration model, they are found to be λ_s = 1.28000, λ_p=1.18766, and λ_d=1.18497. In the 24-configuration model, the parameters λ_{nl} are found to be λ_{1s} = 1.41650, λ_{2s} = 1.27118, λ_{2p} = 1.20150, λ_{3s} = 1.18512, λ_{3p} = 1.14294, λ_{3d} = 1.20426, λ_{4s} = 1.18182, λ_{4p} = 1.14344, λ_{4d} = 1.19724, λ_{4f} = 1.19700. The relativistic corrections are included by using the Breit-Pauli Hamiltonian as a perturbation to the nonrelativistic Hamiltonian. Energy levels, oscillator strengths, and radiative transition rates are calculated in intermediate coupling. The calculated energies for Ca XIII are listed in Table 1 along with experimentally determined energies from Edlen (1983), Feldman et al. (2000), Acton et al. (1985), Doschek et al. (1973) and Fawcett & Hayes (1975). We use the calculated energies and the wave functions to calculate oscillator strengths and transition rates. The A values depend on the wavelength λ as

$$A_{ij} \propto \frac{S^{\rm d}_{ij}}{\lambda^3_{ij}} \qquad \text{dipole transitions}$$
$$A_{ij} \propto \frac{S^{\rm q}_{ij}}{\lambda^5_{ij}} \qquad \text{quadrupole transitions} \qquad (1)$$

where $S^{\rm e}_{ij}$ and $S^{\rm q}_{ij}$ are the line strengths for dipole and quadrupole transitions. We have corrected A values obtained from Superstructure with observed wavelengths wherever possible.

The scattering problem is carried out in the distorted wave approximation using the programs described by Eissner & Seaton (1972) and Eissner (1998). The reactance matrices at incident energies 40, 80, 120, 160 and 200 Ry are calculated in LS coupling. The collision strengths in intermediate coupling are calculated by using these reactance matrices and term-coupling coefficients obtained from structure calculations in the program JAJOM developed by Saraph (1978) and modified by Saraph & Eissner (2005) to calculate collision strengths below the thresholds as well. The distorted wave calculations are carried out for a finite number of incident partial waves and contribution from higher partial waves is calculated in the Coulomb-Bethe approximation using the program of Burgess & Sheorey (1974). The Ca XIII collision strengths Ω_{ij}, transition rates A_{ji}, and $g_i f_{ij}$ (absorption oscillator strengths multiplied by the statistical weight g_i of the lower level) are given in Table 2.

The electron impact excitation rate coefficients (in $\rm cm^3\ s^{-1}$) are obtained by averaging the collision strengths over the Maxwellian electron velocity distribution

$$C^{\rm e}_{ij} = \frac{8.63\times10^{-6}}{g_i T_{\rm e}^{1/2}} \int_{\Delta E_{ij}}^{\infty} \Omega_{ij}(E_i) {\rm e}^{-\frac{E_i}{kT_{\rm e}}} {\rm d}\left(\frac{E_i}{kT_{\rm e}}\right) \qquad (2)$$

where $T_{\rm e}$ is the electron temperature in Kelvin, ΔE_{ij} is the transition energy of the $i \rightarrow j$ transition, E_i is the incident energy with respect to the level i, and k is the Boltzmann constant. The deexcitation rates are given by the principle of detailed balance:

$$C^{\rm d}_{ji} = \frac{g_i}{g_j} {\rm e}^{\frac{\Delta E_{ij}}{kT_{\rm e}}} C^{e}_{ij}. \qquad (3)$$

Table 1. Calculated and observed Ca XIII energy levels. E_{24}: energies calculated using the 24-configuration model; E_6: energies calculated using the 6-configuration model; E_{obs}: observed energies from Edlen (1983 – E), Feldman et al. (2000 – C), Acton et al. (1985 – A), Doschek et al. (1973 – D) and Fawcett & Hayes (1975 – F).

Key	Configuration	Term	E_{24}	E_6	E_{obs}	Ref.
1	$2s^2 2p^4$	$^3P_2$	0	0	0	
2	$2s^2 2p^4$	$^3P_1$	25 016	25 005	24 465	E
3	$2s^2 2p^4$	$^3P_0$	29 488	29 280	28 880	E
4	$2s^2 2p^4$	$^1D_2$	91 945	91 629	88 202	C
5	$2s^2 2p^4$	$^1S_0$	180 687	176 046	178 619	C
6	$2s2p^5$	$^3P_2$	628 533	628 352	618 280	E
7	$2s2p^5$	$^3P_1$	648 949	649 088	638 266	E
8	$2s2p^5$	$^3P_0$	661 061	661 369	650 149	E
9	$2s2p^5$	$^1P_1$	869 796	874 869	850 299	E
10	$2p^6$	$^1S_0$	1 474 925	1 494 094	1 440 313	E
11	$2s^2 2p^3(^4S)3s$	$^5S_2$	3 332 414	3 334 694	3 334 445	A
12	$2s^2 2p^3(^4S)3s$	$^3S_1$	3 373 576	3 374 092	3 374 623	D
13	$2s^2 2p^3(^2D)3s$	$^3D_1$	3 452 104	3 454 808	3 452 799	D
14	$2s^2 2p^3(^2D)3s$	$^3D_2$	3 453 109	3 455 678	3 454 451	D
15	$2s^2 2p^3(^2D)3s$	$^3D_3$	3 459 719	3 459 557	3 458 293	D
16	$2s^2 2p^3(^2D)3s$	$^1D_2$	3 476 606	3 476 903	3 474 589	D
17	$2s^2 2p^3(^4S)3p$	$^5P_1$	3 492 945	3 495 106		
18	$2s^2 2p^3(^4S)3p$	$^5P_2$	3 494 826	3 496 982		
19	$2s^2 2p^3(^4S)3p$	$^5P_3$	3 499 022	3 501 314		
20	$2s^2 2p^3(^4S)3p$	$^3P_1$	3 532 553	3 535 405		
21	$2s^2 2p^3(^2P)3s$	$^3P_0$	3 513 600	3 535 970		
22	$2s^2 2p^3(^4S)3p$	$^3P_2$	3 535 546	3 537 347		
23	$2s^2 2p^3(^2P)3s$	$^3P_1$	3 516 601	3 538 319		
24	$2s^2 2p^3(^4S)3p$	$^3P_0$	3 536 793	3 539 246		
25	$2s^2 2p^3(^2P)3s$	$^3P_2$	3 526 317	3 545 578	3 541 718	D
26	$2s^2 2p^3(^2P)3s$	$^1P_1$	3 541 869	3 561 785	3 564 769	D
27	$2s^2 2p^3(^2D)3p$	$^3D_1$	3 592 977	3 600 620		
28	$2s^2 2p^3(^2D)3p$	$^3D_2$	3 605 070	3 608 939		
29	$2s^2 2p^3(^2D)3p$	$^3D_3$	3 612 093	3 613 805		
30	$2s^2 2p^3(^2D)3p$	$^3F_2$	3 616 355	3 616 754		
31	$2s^2 2p^3(^2D)3p$	$^1P_1$	3 612 136	3 617 342		
32	$2s^2 2p^3(^2D)3p$	$^3F_3$	3 621 835	3 621 614		
33	$2s^2 2p^3(^2D)3p$	$^3F_4$	3 627 680	3 624 862		
34	$2s^2 2p^3(^2D)3p$	$^1F_3$	3 629 169	3 627 858		
35	$2s^2 2p^3(^2D)3p$	$^3P_0$	3 665 245	3 669 940		
36	$2s^2 2p^3(^2D)3p$	$^3P_1$	3 659 430	3 671 676		
37	$2s^2 2p^3(^2D)3p$	$^3P_2$	3 677 036	3 682 448		
38	$2s^2 2p^3(^2P)3p$	$^3D_2$	3 682 754	3 696 081		
39	$2s^2 2p^3(^2P)3p$	$^1P_1$	3 677 765	3 696 187		
40	$2s^2 2p^3(^4S)3d$	$^5D_0$	3 698 189	3 698 959		
41	$2s^2 2p^3(^4S)3d$	$^5D_1$	3 698 362	3 699 001		
42	$2s^2 2p^3(^4S)3d$	$^5D_2$	3 698 628	3 699 060		
43	$2s^2 2p^3(^4S)3d$	$^5D_3$	3 699 002	3 699 170		
44	$2s^2 2p^3(^4S)3d$	$^5D_4$	3 699 764	3 699 626		
45	$2s^2 2p^3(^2P)3p$	$^3S_1$	3 683 480	3 700 931		
46	$2s^2 2p^3(^2P)3p$	$^3P_2$	3 713 781	3 705 292		
47	$2s^2 2p^3(^2P)3p$	$^3D_3$	3 690 721	3 708 687		
48	$2s^2 2p^3(^2P)3p$	$^3D_1$	3 699 898	3 716 819		
49	$2s^2 2p^3(^2D)3p$	$^1D_2$	3 691 124	3 734 783		
50	$2s^2 2p^3(^2P)3p$	$^3P_1$	3 716 373	3 740 644		

Table 1. continued.

Key	Configuration	Term	E_{24}	E_6	E_{obs}	Ref.
51	$2s^22p^3(^2P)3p$	$^3P_0$	3 716 857	3 742 186		
52	$2s^22p^3(^4S)3d$	$^3D_2$	3 741 732	3 742 760	3 739 175	F
53	$2s^22p^3(^4S)3d$	$^3D_1$	3 744 680	3 745 394		
54	$2s^22p^3(^4S)3d$	$^3D_3$	3 745 844	3 746 211	3 742 655	F
55	$2s^22p^3(^2P)3p$	$^1D_2$	3 750 851	3 765 729		
56	$2s^22p^3(^2D)3d$	$^3F_2$	3 802 456	3 806 049		
57	$2s^22p^3(^2D)3d$	$^3F_3$	3 808 179	3 810 136	3 798 959	F
58	$2s^22p^3(^2D)3d$	$^1S_0$	3 811 660	3 812 704		
59	$2s^22p^3(^2D)3d$	$^3F_4$	3 814 745	3 814 904		
60	$2s^22p^3(^2D)3d$	$^3G_3$	3 820 569	3 819 669		
61	$2s^22p^3(^2D)3d$	$^3G_4$	3 823 852	3 821 951		
62	$2s^22p^3(^2D)3d$	$^3G_5$	3 828 150	3 824 258		
63	$2s^22p^3(^2D)3d$	$^1G_4$	3 830 981	3 827 910		
64	$2s^22p^3(^2D)3d$	$^3D_1$	3 829 217	3 832 957	3 827 839	F
65	$2s^22p^3(^2P)3p$	$^1S_0$	3 811 460	3 835 779		
66	$2s^22p^3(^2D)3d$	$^3D_2$	3 842 455	3 844 495	3 838 493	F
67	$2s^22p^3(^2D)3d$	$^1P_1$	3 845 728	3 845 969		
68	$2s^22p^3(^2D)3d$	$^3D_3$	3 847 896	3 847 882	3 841 278	F
69	$2s^22p^3(^2D)3d$	$^3P_2$	3 855 688	3 856 487	3 849 559	F
70	$2s^22p^3(^2D)3d$	$^3P_0$	3 858 304	3 858 753		
71	$2s^22p^3(^2D)3d$	$^3P_1$	3 860 125	3 860 140		
72	$2s^22p^3(^2P)3d$	$^1D_2$	3 852 481	3 861 307		
73	$2s^22p^3(^2D)3d$	$^3S_1$	3 866 067	3 868 332	3 863 988	F
74	$2s^22p^3(^2P)3d$	$^3F_3$	3 883 656	3 888 405	3 879 502	F
75	$2s^22p^3(^2P)3d$	$^3F_2$	3 887 217	3 904 618		
76	$2s^22p^3(^2D)3d$	$^1F_3$	3 889 915	3 906 097	3 894 991	F
77	$2s^22p^3(^2P)3d$	$^3F_4$	3 890 947	3 907 674		
78	$2s^22p^3(^2P)3d$	$^3P_0$	3 892 282	3 913 144		
79	$2s^22p^3(^2P)3d$	$^3P_1$	3 896 347	3 914 793		
80	$2s^22p^3(^2P)3d$	$^3P_2$	3 897 020	3 914 874		
81	$2s^22p^3(^2P)3d$	$^3D_2$	3 908 234	3 925 811	3 914 002	F
82	$2s^22p^3(^2P)3d$	$^3D_3$	3 915 250	3 931 801	3 916 960	F
83	$2s^22p^3(^2P)3d$	$^3D_1$	3 914 204	3 933 419	3 923 871	F
84	$2s^22p^3(^2D)3d$	$^1D_2$	3 931 725	3 944 741		
85	$2s^22p^3(^2P)3d$	$^1F_3$	3 935 281	3 952 838		
86	$2s^22p^3(^2P)3d$	$^1P_1$	3 972 703	3 993 076	3 992 410	F

In order to carry out the integration in Eq. (2), it is necessary to know the collision strength Ω across the whole energy range, from threshold to infinity. However, the present theoretical calculations only provide collision strengths for five energy values, so some interpolation/extrapolation technique is required in order to properly take into account the energy dependence of the collision strength. In the present work we have adopted the method described by Burgess & Tully (1992) to extrapolate the collision strengths to the high- and low-energy limit. This method has been used recently by Bhatia et al. (2003) and details are given there.

3. Level populations and relative line intensities

The steady state level populations are obtained by solving the equations

$$\frac{dN_i}{dt} = -N_e N_i \left(\sum_{j>i} C^e_{ij} + \sum_{j<i} C^d_{ij} \right) + \sum_{j>i} N_j A_{ji} - N_i \sum_{j<i} A_{ij} + N_e \left(\sum_{j>i} N_j C^d_{ji} + \sum_{j<i} N_j C^e_{ji} \right)$$

$$\frac{dN_i}{dt} = 0 \qquad (4)$$

Table 2. Weighted oscillator strengths (dimensionless), A values (s^{-1}) and collision strengths (dimensionless) for Ca XIII as a function of incident electron energies. Weighted oscillator strengths are obtained multiplying the absorption oscillator strength f_{ij} with the statistical weight g_i of the lower level i. The full table is available in electronic form at the CDS.

i	j	$g_i f_{ij}$	A_{ij}	Collision strengths				
				40 Ry	80 Ry	120 Ry	160 Ry	200 Ry
1	2		3.418E+02	5.984E−02	4.672E−02	4.203E−02	3.993E−02	3.889E−02
1	3		1.341E−02	1.783E−02	1.670E−02	1.665E−02	1.680E−02	1.696E−02
1	4		8.411E+02	5.249E−02	2.881E−02	1.966E−02	1.522E−02	1.275E−02
1	5		1.300E+00	5.447E−03	2.462E−03	1.401E−03	9.234E−04	6.744E−04
1	6	4.263E−01	2.245E+10	1.171E+00	1.370E+00	1.502E+00	1.600E+00	1.678E+00
1	7	1.531E−01	1.434E+10	4.046E−01	4.715E−01	5.163E−01	5.499E−01	5.765E−01
1	8		3.637E+01	9.200E−04	4.921E−04	3.074E−04	2.116E−04	1.555E−04
1	9	1.512E−02	2.573E+09	3.442E−02	3.522E−02	3.658E−02	3.799E−02	3.931E−02
1	10		1.049E+04	2.709E−04	1.397E−04	9.490E−05	7.518E−05	6.493E−05
1	11	2.445E−03	3.628E+09	4.666E−03	2.120E−03	1.320E−03	9.813E−04	8.200E−04
1	12	2.313E−01	5.854E+11	7.354E−03	1.690E−02	2.505E−02	3.165E−02	3.712E−02
1	13	4.722E−03	1.253E+10	1.220E−03	7.789E−04	7.227E−04	7.514E−04	8.042E−04
1	14	9.491E−02	1.512E+11	4.049E−03	7.126E−03	1.011E−02	1.260E−02	1.471E−02
1	15	2.520E−01	2.873E+11	9.216E−03	1.865E−02	2.702E−02	3.389E−02	3.964E−02

where N_j is the number density of level j, N_e is the electron density, and A_{ji} (s^{-1}) is the spontaneous radiative transition rate from level j to level i. The equations have been solved at several electron densities, $\log N_e(cm^{-3}) = 8$, 9, 10, 11, 12, 13, and 14. The fractional populations $n_j = N_j/N_T$ at $\log T_e = 6.5$, where N_T is the sum of the number density of all the Ca XIII levels, are listed in Table 3 and intensities of various lines at $\log T_e = 6.5$, the temperature of maximum abundance of Ca XIII (Mazzotta et al. 1998), are given in Table 4. The intensity of an optically thin line for a radiative transition from level j to level i is given by $I_{ji} = n_j A_{ji}$ in photon units.

4. Comparison with earlier work

We have compared the present results to transition rates calculated by other authors in the past. These calculations have been carried out using the same computer codes and approximations as in the present work (Mason 1975; Baliyan & Bhatia 1993, 1994; Galavis et al. 1997) and with different methods (Tachiev & Froese Fischer 2002; Baluja & Zeippen 1988; Froese Fischer & Saha 1983; Cheng et al. 1979; Zhang & Sampson 2002; Fawcett 1986; Gaigalas et al. 1994; Vilkas et al. 1994). Of all the works listed here, only Mason (1975), Zhang & Sampson (1992) and Baliyan & Bhatia (1994) provide collision rates, while all the rest published only radiative data. Calculations have been carried out with atomic models different from those used in the present work, so their comparison with our results will help us to understand the effect of including a larger number of configurations in the atomic model. To this respect, we also compared our 6-configuration calculation with the more elaborated 24-configuration one. It is worth noting that Fawcett (1986) reports only weighted oscillator strengths gf: for the present comparison, we have calculated A values using his gf values and the theoretical wavelengths resulting from his calculation.

A comparison of A values from different calculations is reported in Table 5. A values for transitions within the ground configurations from all authors show excellent agreement, within 10%, with only few exceptions. Slightly larger disagreements are found with the results from Cheng et al. (1979) and Mason (1975) due to the limitations of their atomic models, but differences are lower than 30%, and occur mostly for transitions of little importance for the population of the upper level.

Allowed transitions within the $n = 2$ complex are in excellent agreement when we consider the results of Tachiev & Froese Fischer (2002), Vilkas et al. (1994) and the present 24-configuration calculation. This is as expected since these three computations have been carried out using more sophisticated atomic models than the others. This result shows that an atomic model that includes all the relevant configurations to take into account configuration interaction is necessary, and that different methods and approximations lead to similar results. The other calculations usually provide higher results, and they show various levels of disagreement among themselves and with the three calculations mentioned above.

A few authors have calculated radiative data for transitions from the $2s^2 2p^3 3l$ ($l = s, p, d$) levels, and their results, given in Table 5 for the transitions corresponding to observed lines, show some disagreement. Results from the present 24-configuration calculation and Tachiev & Froese Fischer (2002) usually agree within 20%, but for some transitions show large disagreements, up to a maximum of a factor 2 in one case. Results from the 6-configuration calculation and Fawcett (1986) show a somehow worse agreement in a few cases, while for some transitions compare favorably with the other calculations.

A comparison of collision strengths between the present calculation (6-configuration model) and those from Zhang & Sampson (2002) has been done for all transitions within the $n = 2$ complex. Collision strengths are provided at energies different from those used in the present calculation, but their behavior as a function of energy show excellent agreement between the two calculations. The only exceptions are for the transitions from the $^3P_0$ and $^1S_0$ levels in the ground

Table 3. Level populations for Ca XIII.

Key	Population						
	8	9	10	11	12	13	14
1	9.976(−01)	9.806(−01)	9.274(−01)	8.241(−01)	6.001(−01)	4.474(−01)	4.036(−01)
2	1.417(−04)	1.356(−03)	1.167(−02)	8.237(−02)	2.215(−01)	2.345(−01)	2.144(−01)
3	2.235(−03)	1.785(−02)	5.932(−02)	7.848(−02)	8.041(−02)	7.295(−02)	6.873(−02)
4	1.606(−05)	1.602(−04)	1.581(−03)	1.482(−02)	9.545(−02)	2.253(−01)	2.749(−01)
5	1.413(−07)	1.469(−06)	1.630(−05)	1.857(−04)	2.552(−03)	1.987(−02)	3.842(−02)
6	2.771(−12)	2.727(−11)	2.599(−10)	2.432(−09)	2.053(−08)	1.676(−07)	1.531(−06)
7	9.112(−13)	9.509(−12)	1.055(−10)	1.092(−09)	1.027(−08)	8.878(−08)	8.226(−07)
8	4.455(−15)	6.070(−14)	1.861(−12)	1.012(−10)	2.637(−09)	2.806(−08)	2.582(−07)
9	3.387(−14)	3.373(−13)	3.409(−12)	4.372(−11)	1.104(−09)	2.285(−08)	2.798(−07)
10	1.885(−16)	1.892(−15)	1.926(−14)	2.121(−13)	3.230(−12)	5.181(−11)	6.109(−10)
11	2.265(−13)	2.257(−12)	2.229(−11)	2.156(−10)	1.902(−09)	1.569(−08)	1.427(−07)
12	8.109(−16)	8.140(−15)	8.217(−14)	8.173(−13)	7.611(−12)	6.550(−11)	6.048(−10)
13	2.107(−16)	2.334(−15)	2.983(−14)	3.705(−13)	4.748(−12)	5.009(−11)	4.930(−10)
14	9.560(−16)	9.518(−15)	9.439(−14)	9.704(−13)	1.044(−11)	1.065(−10)	1.053(−09)
15	3.467(−15)	3.411(−14)	3.244(−13)	2.990(−12)	2.588(−11)	2.491(−10)	2.487(−09)
16	7.195(−16)	7.114(−15)	6.905(−14)	6.969(−13)	9.126(−12)	1.345(−10)	1.516(−09)
17	6.010(−14)	6.053(−13)	6.159(−12)	6.124(−11)	5.617(−10)	4.718(−09)	4.303(−08)
18	1.626(−13)	1.618(−12)	1.595(−11)	1.565(−10)	1.432(−09)	1.199(−08)	1.090(−07)
19	3.374(−13)	3.357(−12)	3.301(−11)	3.157(−10)	2.716(−09)	2.216(−08)	2.014(−07)
20	4.506(−14)	4.502(−13)	4.553(−12)	5.161(−11)	6.163(−10)	5.693(−09)	5.222(−08)
21	1.380(−17)	1.599(−16)	2.529(−15)	6.212(−14)	1.334(−12)	1.462(−11)	1.403(−10)
22	1.873(−13)	1.851(−12)	1.784(−11)	1.649(−10)	1.326(−09)	1.056(−08)	9.635(−08)
23	5.078(−16)	5.341(−15)	6.045(−14)	6.431(−13)	6.654(−12)	6.683(−11)	6.650(−10)
24	1.628(−14)	1.855(−13)	2.453(−12)	2.693(−11)	2.563(−10)	2.242(−09)	2.090(−08)
25	7.076(−16)	7.029(−15)	6.963(−14)	7.506(−13)	9.509(−12)	1.161(−10)	1.234(−09)
26	1.503(−16)	1.497(−15)	1.496(−14)	1.672(−13)	2.786(−12)	4.847(−11)	5.893(−10)
27	1.467(−14)	1.474(−13)	1.496(−12)	1.564(−11)	1.714(−10)	1.776(−09)	1.765(−08)
28	4.527(−14)	4.496(−13)	4.415(−12)	4.378(−11)	4.502(−10)	4.766(−09)	4.832(−08)
29	1.129(−13)	1.112(−12)	1.060(−11)	9.986(−11)	9.606(−10)	1.052(−08)	1.095(−07)
30	1.530(−14)	1.614(−13)	1.855(−12)	2.124(−11)	2.560(−10)	2.754(−09)	2.753(−08)
31	8.799(−15)	8.831(−14)	8.949(−13)	9.335(−12)	1.062(−10)	1.194(−09)	1.228(−08)
32	3.567(−14)	3.614(−13)	3.765(−12)	4.115(−11)	4.933(−10)	5.454(−09)	5.522(−08)
33	2.307(−13)	2.269(−12)	2.159(−11)	2.007(−10)	1.799(−09)	1.793(−08)	1.808(−07)
34	1.270(−13)	1.258(−12)	1.222(−11)	1.188(−10)	1.213(−09)	1.344(−08)	1.393(−07)
35	6.217(−16)	1.323(−14)	3.186(−13)	4.033(−12)	4.084(−11)	3.726(−10)	3.529(−09)
36	1.581(−15)	1.617(−14)	2.026(−13)	5.116(−12)	1.122(−10)	1.177(−09)	1.089(−08)
37	5.832(−14)	5.734(−13)	5.428(−12)	4.842(−11)	3.587(−10)	2.753(−09)	2.516(−08)
38	5.116(−14)	5.038(−13)	4.798(−12)	4.369(−11)	3.676(−10)	3.570(−09)	3.612(−08)
39	9.430(−16)	1.078(−14)	1.473(−13)	2.005(−12)	2.958(−11)	3.543(−10)	3.740(−09)
40	1.515(−15)	1.551(−14)	1.649(−13)	1.695(−12)	1.618(−11)	1.385(−10)	1.267(−09)
41	4.698(−15)	4.765(−14)	4.942(−13)	5.010(−12)	4.728(−11)	4.021(−10)	3.672(−09)
42	1.115(−14)	1.116(−13)	1.118(−12)	1.114(−11)	1.042(−10)	8.812(−10)	8.026(−09)
43	5.296(−14)	5.260(−13)	5.156(−12)	5.035(−11)	4.582(−10)	3.824(−09)	3.476(−08)
44	1.156(−13)	1.149(−12)	1.126(−11)	1.067(−10)	9.001(−10)	7.274(−09)	6.609(−08)
45	3.764(−16)	4.085(−15)	5.418(−14)	1.056(−12)	2.098(−11)	2.501(−10)	2.606(−09)
46	6.763(−14)	6.697(−13)	6.481(−12)	5.995(−11)	5.074(−10)	4.743(−09)	4.713(−08)
47	1.383(−14)	1.381(−13)	1.385(−12)	1.474(−11)	1.741(−10)	2.058(−09)	2.251(−08)
48	1.252(−15)	1.286(−14)	1.472(−13)	2.438(−12)	4.391(−11)	4.843(−10)	4.751(−09)
49	9.572(−14)	9.412(−13)	8.914(−12)	7.967(−11)	5.931(−10)	4.576(−09)	4.210(−08)
50	1.267(−15)	1.522(−14)	3.400(−13)	1.544(−11)	3.907(−10)	4.144(−09)	3.814(−08)

Table 3. continued.

Key	Population						
	8	9	10	11	12	13	14
51	4.235(−16)	2.611(−14)	8.427(−13)	1.118(−11)	1.162(−10)	1.066(−09)	1.009(−08)
52	4.081(−16)	4.050(−15)	4.007(−14)	4.320(−13)	4.803(−12)	4.326(−11)	3.953(−10)
53	7.933(−17)	9.771(−16)	1.488(−14)	1.935(−13)	2.369(−12)	2.258(−11)	2.125(−10)
54	1.221(−15)	1.202(−14)	1.144(−13)	1.032(−12)	7.829(−12)	6.018(−11)	5.462(−10)
55	7.782(−15)	7.882(−14)	8.692(−13)	1.564(−11)	5.764(−10)	1.255(−08)	1.518(−07)
56	8.246(−16)	8.233(−15)	8.240(−14)	8.645(−13)	1.002(−11)	1.128(−10)	1.157(−09)
57	1.440(−15)	1.425(−14)	1.381(−13)	1.320(−12)	1.284(−11)	1.383(−10)	1.427(−09)
58	2.139(−15)	2.134(−14)	2.119(−13)	2.102(−12)	2.008(−11)	1.817(−10)	1.718(−09)
59	5.466(−14)	5.379(−13)	5.129(−12)	4.868(−11)	4.892(−10)	5.652(−09)	5.981(−08)
60	1.159(−15)	1.186(−14)	1.262(−13)	1.357(−12)	1.524(−11)	1.598(−10)	1.591(−09)
61	2.603(−14)	2.650(−13)	2.797(−12)	3.061(−11)	3.654(−10)	4.051(−09)	4.109(−08)
62	6.525(−14)	6.418(−13)	6.103(−12)	5.684(−11)	5.122(−10)	5.104(−09)	5.137(−08)
63	4.130(−14)	4.086(−13)	3.961(−12)	3.825(−11)	3.765(−10)	3.976(−09)	4.051(−08)
64	5.435(−17)	6.701(−16)	1.010(−14)	1.205(−13)	1.406(−12)	1.595(−11)	1.646(−10)
65	1.255(−16)	1.268(−15)	1.324(−14)	1.626(−13)	4.680(−12)	2.461(−10)	4.562(−09)
66	3.881(−17)	3.984(−16)	5.066(−15)	1.307(−13)	2.897(−12)	3.060(−11)	2.834(−10)
67	7.714(−17)	8.072(−16)	9.115(−15)	1.052(−13)	1.348(−12)	1.640(−11)	1.779(−10)
68	9.271(−16)	9.115(−15)	8.630(−14)	7.695(−13)	5.693(−12)	4.360(−11)	3.981(−10)
69	1.038(−15)	1.021(−14)	9.678(−14)	8.712(−13)	6.611(−12)	5.094(−11)	4.630(−10)
70	6.663(−18)	7.138(−17)	1.049(−15)	3.152(−14)	7.279(−13)	7.692(−12)	7.104(−11)
71	1.529(−16)	1.594(−15)	1.780(−14)	1.987(−13)	2.186(−12)	2.030(−11)	1.915(−10)
72	5.268(−17)	5.260(−16)	5.283(−15)	5.823(−14)	9.188(−13)	1.455(−11)	1.655(−10)
73	2.965(−16)	2.925(−15)	2.803(−14)	2.604(−13)	2.146(−12)	1.746(−11)	1.605(−10)
74	4.454(−16)	4.384(−15)	4.182(−14)	3.979(−13)	4.453(−12)	6.087(−11)	6.775(−10)
75	5.570(−17)	6.401(−16)	8.969(−15)	1.368(−13)	2.450(−12)	3.337(−11)	3.641(−10)
76	2.059(−16)	2.044(−15)	1.992(−14)	1.863(−13)	1.587(−12)	1.447(−11)	1.427(−10)
77	2.060(−14)	2.060(−13)	2.071(−12)	2.201(−11)	2.623(−10)	3.201(−09)	3.556(−08)
78	2.410(−18)	2.694(−17)	4.716(−16)	1.747(−14)	4.262(−13)	4.603(−12)	4.344(−11)
79	1.633(−17)	2.797(−16)	6.037(−15)	8.938(−14)	1.218(−12)	1.259(−11)	1.245(−10)
80	1.757(−16)	1.775(−15)	1.874(−14)	2.389(−13)	3.495(−12)	4.003(−11)	4.169(−10)
81	1.067(−16)	1.064(−15)	1.092(−14)	1.460(−13)	2.235(−12)	2.367(−11)	2.279(−10)
82	1.472(−15)	1.447(−14)	1.372(−13)	1.230(−12)	9.294(−12)	7.331(−11)	6.801(−10)
83	1.141(−17)	2.424(−16)	6.016(−15)	9.377(−14)	1.318(−12)	1.329(−11)	1.280(−10)
84	2.529(−17)	2.542(−16)	2.760(−15)	4.707(−14)	1.092(−12)	1.677(−11)	1.853(−10)
85	1.118(−17)	1.141(−16)	1.288(−15)	2.413(−14)	9.079(−13)	1.979(−11)	2.393(−10)
86	7.205(−18)	1.204(−16)	2.493(−15)	3.126(−14)	3.658(−13)	6.320(−12)	9.170(−11)

configuration to the singlet $2p^6\ ^1S_0$ level, where there is a disagreement of a factor 1.5–2.

Baliyan & Bhatia (1994) calculated collision strengths in LS coupling for $n = 2 \rightarrow 2$ and $n = 2 \rightarrow 3$ transitions using the R-Matrix approximation, which takes into account resonances. They provide collision strengths in LS coupling, so a comparison with the present results can only be done by splitting the Baliyan & Bhatia (1994) results according to statistical weights. We also compared our results in LS coupling with those of Baliyan & Bhatia (1994). In LS coupling, results show excellent agreement, within 10%. However, the comparison of fine-structure collision strengths obtained by splitting the Baliyan & Bhatia (1994) results according to statistical weights with our results shows large disagreements: differences can rise up to 50-70% for allowed transitions, and orders of magnitude for forbidden transitions. In general, splitting collision strengths according to statistical weights does not provide accurate results.

Some comments are needed on the limitations of the distorted wave approximation when applied to O-like systems. Butler & Zeippen (2001) and Gu (2003) carried out extensive calculations of collision rates for Fe XIX including resonances, which have been neglected from all calculations of Ca XIII collision rates available in the literature, as well as in the present one.

Butler & Zeippen (2001) demonstrate that resonances are very important for collisional excitation. By inspecting their collision strengths as a function of electron energy, resonances

Table 4. Emissivities of the strongest lines emitted by Ca XIII. Units are phot s^{-1}. The "−" sign before wavelengths indicates that they have been calculated using theoretical energy levels.

Transition	Wavelength (Å)	Emissivity (phot s^{-1})						
		8	9	10	11	12	13	14
1−82	25.530	1.49(−03)	1.47(−02)	1.39(−01)	1.25(+00)	9.43(+00)	7.44(+01)	6.90(+02)
3−83	25.674	3.28(−05)	6.97(−04)	1.73(−02)	2.69(−01)	3.79(+00)	3.82(+01)	3.68(+02)
2−81	25.710	3.00(−04)	2.99(−03)	3.07(−02)	4.10(−01)	6.27(+00)	6.65(+01)	6.40(+02)
1−73	25.880	1.36(−03)	1.34(−02)	1.28(−01)	1.19(+00)	9.82(+00)	7.99(+01)	7.35(+02)
1−72	−25.957	1.43(−04)	1.43(−03)	1.44(−02)	1.59(−01)	2.50(+00)	3.96(+01)	4.51(+02)
4−84	−26.043	1.05(−04)	1.06(−03)	1.15(−02)	1.96(−01)	4.55(+00)	6.99(+01)	7.72(+02)
2−71	−26.075	2.79(−04)	2.91(−03)	3.25(−02)	3.62(−01)	3.99(+00)	3.70(+01)	3.49(+02)
2−66	26.219	1.12(−04)	1.15(−03)	1.46(−02)	3.77(−01)	8.36(+00)	8.84(+01)	8.18(+02)
5−86	26.219	4.82(−05)	8.06(−04)	1.67(−02)	2.09(−01)	2.45(+00)	4.23(+01)	6.14(+02)
4−74	26.376	5.83(−04)	5.74(−03)	5.48(−02)	5.21(−01)	5.83(+00)	7.97(+01)	8.87(+02)
4−69	26.586	7.35(−04)	7.23(−03)	6.85(−02)	6.17(−01)	4.68(+00)	3.61(+01)	3.28(+02)
1−54	26.719	1.79(−03)	1.76(−02)	1.68(−01)	1.51(+00)	1.15(+01)	8.82(+01)	8.01(+02)
2−52	26.920	3.45(−04)	3.42(−03)	3.39(−02)	3.65(−01)	4.06(+00)	3.66(+01)	3.34(+02)
2−25	28.431	1.05(−04)	1.04(−03)	1.03(−02)	1.11(−01)	1.41(+00)	1.72(+01)	1.82(+02)
1−15	28.916	1.08(−03)	1.07(−02)	1.01(−01)	9.35(−01)	8.09(+00)	7.79(+01)	7.78(+02)
4−16	29.530	4.97(−04)	4.91(−03)	4.77(−02)	4.81(−01)	6.30(+00)	9.29(+01)	1.05(+03)
1−12	29.633	4.86(−04)	4.88(−03)	4.92(−02)	4.90(−01)	4.56(+00)	3.92(+01)	3.62(+02)
1−11	29.990	1.01(−03)	1.00(−02)	9.92(−02)	9.60(−01)	8.47(+00)	6.99(+01)	6.36(+02)
2−11	30.212	1.50(−04)	1.50(−03)	1.48(−02)	1.43(−01)	1.26(+00)	1.04(+01)	9.46(+01)
6−37	−32.803	2.10(−03)	2.06(−02)	1.95(−01)	1.74(+00)	1.29(+01)	9.91(+01)	9.06(+02)
6−38	−32.962	6.25(−04)	6.15(−03)	5.86(−02)	5.33(−01)	4.49(+00)	4.36(+01)	4.41(+02)
6−36	−32.994	4.76(−05)	4.87(−04)	6.10(−03)	1.54(−01)	3.38(+00)	3.54(+01)	3.28(+02)
1−9	117.606	7.56(−05)	7.53(−04)	7.61(−03)	9.76(−02)	2.47(+00)	5.10(+01)	6.25(+02)
4−9	131.217	2.98(−03)	2.96(−02)	3.00(−01)	3.84(+00)	9.71(+01)	2.01(+03)	2.46(+04)
5−9	148.828	2.14(−04)	2.13(−03)	2.15(−02)	2.76(−01)	6.98(+00)	1.44(+02)	1.77(+03)
1−7	156.675	1.19(−02)	1.25(−01)	1.38(+00)	1.43(+01)	1.35(+02)	1.16(+03)	1.08(+04)
2−8	159.825	1.30(−04)	1.77(−03)	5.43(−02)	2.95(+00)	7.70(+01)	8.19(+02)	7.53(+03)
1−6	161.739	5.68(−02)	5.59(−01)	5.33(+00)	4.99(+01)	4.21(+02)	3.43(+03)	3.14(+04)
2−7	162.920	6.23(−03)	6.50(−02)	7.22(−01)	7.47(+00)	7.03(+01)	6.07(+02)	5.63(+03)
3−7	164.100	7.96(−03)	8.30(−02)	9.21(−01)	9.54(+00)	8.97(+01)	7.75(+02)	7.18(+03)
2−6	168.403	1.72(−02)	1.69(−01)	1.61(+00)	1.51(+01)	1.27(+02)	1.04(+03)	9.50(+03)
4−6	188.652	1.01(−03)	9.92(−03)	9.46(−02)	8.85(−01)	7.47(+00)	6.10(+01)	5.57(+02)
16−55	−364.638	3.40(−05)	3.45(−04)	3.80(−03)	6.84(−02)	2.52(+00)	5.49(+01)	6.64(+02)
26−55	−478.509	1.40(−05)	1.42(−04)	1.57(−03)	2.82(−02)	1.04(+00)	2.26(+01)	2.74(+02)
29−59	−493.458	1.19(−04)	1.17(−03)	1.11(−02)	1.06(−01)	1.06(+00)	1.23(+01)	1.30(+02)
32−61	−495.009	8.98(−05)	9.15(−04)	9.65(−03)	1.06(−01)	1.26(+00)	1.40(+01)	1.42(+02)
34−63	−495.513	1.38(−04)	1.37(−03)	1.32(−02)	1.28(−01)	1.26(+00)	1.33(+01)	1.36(+02)
19−44	−498.154	3.79(−04)	3.77(−03)	3.69(−02)	3.50(−01)	2.95(+00)	2.39(+01)	2.17(+02)
33−62	−498.828	2.26(−04)	2.22(−03)	2.11(−02)	1.97(−01)	1.77(+00)	1.77(+01)	1.78(+02)
15−33	−595.378	4.98(−04)	4.90(−03)	4.66(−02)	4.34(−01)	3.89(+00)	3.87(+01)	3.91(+02)
11−19	−600.212	6.61(−04)	6.57(−03)	6.46(−02)	6.18(−01)	5.32(+00)	4.34(+01)	3.94(+02)
11−18	−615.720	2.88(−04)	2.87(−03)	2.83(−02)	2.78(−01)	2.54(+00)	2.13(+01)	1.93(+02)
12−22	−617.399	2.87(−04)	2.83(−03)	2.73(−02)	2.52(−01)	2.03(+00)	1.62(+01)	1.47(+02)
2−5	648.680	1.15(−03)	1.20(−02)	1.33(−01)	1.52(+00)	2.08(+01)	1.62(+02)	3.14(+02)
16−34	−655.468	2.03(−04)	2.01(−03)	1.95(−02)	1.90(−01)	1.94(+00)	2.15(+01)	2.22(+02)
15−29	−656.282	1.52(−04)	1.50(−03)	1.43(−02)	1.35(−01)	1.30(+00)	1.42(+01)	1.48(+02)
1−4	1133.758	1.21(−02)	1.20(−01)	1.19(+00)	1.11(+01)	7.17(+01)	1.69(+02)	2.07(+02)
2−4	1568.940	1.56(−03)	1.56(−02)	1.54(−01)	1.44(+00)	9.28(+00)	2.19(+01)	2.67(+01)
1−2	4087.479	4.53(−02)	4.34(−01)	3.74(+00)	2.64(+01)	7.09(+01)	7.50(+01)	6.86(+01)

Table 5. Comparison between the results of the previous work (24C: 24-configuration model; 6C: 6-configuration model) with those from earlier work: Galavis et al. (1997, G97); Baluja & Zeippen (1988, BZ88); Tachiev & Froese Fischer (2002, TFF02); Froese Fischer & Saha (1983, FS83); Gaigalas et al. (1994, G94); Cheng et al. (1979, C79); Mason (1975, M75); Vilkas et al. (1994, V94); Zhang & Sampson (2002, ZS02); Fawcett (1986, F86), Baliyan & Bhatia (1993, BB93).

Transitions within the ground configuration									
Trans	24C	6C	G97	BZ88	TFF02	FS83	G94	C79	M75
1−2	3.200(+2)	3.418(+2)	3.195(+2)	3.213(+2)	3.328(+2)	3.198(+2)	3.099(+2)	3.137(+2)	3.204(−2)
1−3	1.267(−2)	1.341(−2)	1.256(−2)	1.244(−2)	1.221(−2)	1.277(−2)	1.209(−2)	1.182(−2)	1.200(−2)
1−4	7.517(+2)	8.411(+2)	7.858(+2)	7.640(+2)	8.098(+2)	8.087(+2)	7.626(+2)	8.632(+2)	7.978(+2)
1−5	1.484(0)	1.300(0)	1.786(0)	1.687(0)	1.739(0)	1.587(0)	1.612(0)	1.457(0)	1.224(0)
2−3	4.449(0)	4.024(0)	4.453(0)	4.475(0)	3.389(0)	4.263(0)	4.809(0)	4.025(0)	3.915(0)
2−4	9.726(+1)	1.129(+2)	1.018(+2)	9.890(+1)	1.045(+2)	1.074(+2)	1.000(+2)	1.167(+2)	1.059(+2)
2−5	8.160(+3)	8.215(+3)	8.052(+3)	8.095(+3)	8.204(+3)	8.098(+3)	7.725(+3)	8.553(+3)	7.829(+3)
3−4	4.474(−3)	6.420(−3)	4.028(−3)	4.121(−3)		5.430(−3)	4.108(−3)	6.286(−3)	6.000(−3)
4−5	1.265(+1)	9.121(0)	1.277(+1)	1.276(+1)	1.204(+1)	1.213(+1)	1.235(+1)	9.404(0)	8.961(0)
$n = 2 \rightarrow 2$ transitions									
Trans	24C	6C	V94	ZS02	TFF02	F86	BB93	C79	
1−6	2.050(+10)	2.245(+10)	1.934(+10)	2.350(+10)	1.983(+10)	2.149(+10)	2.196(+10)	2.414(+10)	
1−7	1.311(+10)	1.434(+10)	1.234(+10)	1.498(+10)	1.272(+10)	1.375(+10)	1.419(+10)	1.546(+10)	
2−8	2.918(+10)	3.199(+10)	2.750(+10)	3.343(+10)	2.826(+10)	3.053(+10)	3.142(+10)	3.446(+10)	
3−7	8.731(+9)	9.574(+9)	8.272(+9)	9.984(+9)	8.459(+9)	9.251(+9)	9.305(+9)	1.027(+10)	
3−9	1.721(+8)	1.871(+8)	1.497(+8)	2.174(+8)	1.732(+8)		2.741(+8)	2.398(+8)	
4−6	3.639(+8)	4.026(+8)	3.527(+8)	4.102(+8)	3.650(+8)		5.066(+8)	4.571(+8)	
4−9	8.787(+10)	1.044(+11)	8.411(+10)	9.938(+10)	8.558(+10)	9.164(+10)	9.548(+10)	1.046(+11)	
5−9	6.320(+9)	6.864(+9)	6.210(+9)	7.138(+9)	6.274(+9)	7.321(+9)	7.085(+9)	7.706(+9)	
9−10	8.284(+10)	1.071(+11)	7.854(+10)	9.910(+10)	7.950(+10)	8.588(+10)	9.267(+10)	1.067(+11)	
$n = 3 \rightarrow 2$ transitions									
Trans	24C	6C	TFF02	F86	BB93				
1−69	2.541(+12)	4.837(+12)	4.723(+12)	4.880(+12)					
1−68	4.273(+12)	4.065(+12)	4.013(+12)	4.537(+12)					
1−73	4.577(+12)	3.712(+12)	3.833(+12)	4.493(+12)					
1−82	1.015(+12)	1.753(+12)	1.044(+12)	1.200(+12)					
4−69	7.080(+11)	1.745(+10)	7.717(+10)	1.565(+11)					
1−54	1.466(+12)	1.445(+12)	1.447(+12)	1.728(+12)					
1−11	4.453(+9)	3.628(+9)	3.375(+9)		3.812(+9)				
1−15	3.127(+11)	2.873(+11)	3.056(+11)	3.292(+11)	2.761(+11)				
4−16	6.905(+11)	7.124(+11)	6.837(+11)	7.738(+11)	5.818(+11)				
1−12	5.991(+11)	5.854(+11)	5.811(+11)	6.979(+11)	5.577(+11)				
6−37	3.601(+10)	8.588(+9)	2.570(+10)						
7−38	1.221(+10)	1.820(+9)	6.146(+9)						
9−49	7.111(+9)	4.966(+8)	4.776(+9)						

for transitions within the $n = 2$ complex are found at all energies below 80 Ry, so their contribution to the convolution with a maxwellian velocity distribution is very important at all temperatures where Fe XIX abundance is non-negligible. However, resonances for levels in the $2s^2 2p^3 3l$ configurations are limited to energies lower than 8–9 Ry, so their contributions will be important only at low temperatures, where the Fe XIX abundance is low. Gu (2003) showed that the contribution of resonance excitation to the Fe XIX $2s^2 2p^3 3l$ levels is less than 10% for the 3d levels, around 10–15% for the 3p levels and $\simeq$ 30% for the 3s levels at the temperatures where Fe XIX is most abundant.

Although the exact energy position of resonances in Ca XIII cannot be predicted by scaling those in Fe XIX, it is reasonable to expect that, qualitatively, the same results apply to Ca XIII. Therefore, resonances will be very important for collisional excitation of the $n = 2$ complex, but will have a more limited,

Table 6. Comparison between collision strengths from the present calculations with the results of Baliyan & Bhatia (1994 – BB94). The incident electron energy is 120 Ry. Comparison is carried out both in intermediate and LS coupling. Baliyan & Bhatia (1994) LS coupling collision strengths have been splitted into intermediate coupling using statistical weights of levels.

Transition	LS	LS coupling		J values	Intermediate coupling	
		Present	BB94		Present	BB94
1–4	^{3}P–^{1}D	2.713(−2)	2.815(−2)	2–2	1.966(−2)	1.563(−2)
2–4				1–2	1.080(−2)	9.383(−3)
3–4				0–2	4.147(−3)	3.128(−3)
1–5	^{3}P–^{1}S	2.791(−3)	2.611(−3)	2–0	1.401(−3)	1.450(−3)
2–5				1–0	1.310(−3)	8.703(−4)
3–5				0–0	4.079(−4)	2.901(−4)
1–6	^{3}P–^{3}P	3.726(0)	3.837(0)	2–2	1.502(0)	1.184(0)
1–7				2–1	5.163(−1)	7.106(−1)
1–8				2–0	3.074(−4)	2.369(−1)
2–6				1–2	5.214(−1)	7.106(−1)
2–7				1–1	3.089(−1)	4.263(−1)
2–8				1–0	4.082(−1)	1.421(−1)
3–6				0–2	9.161(−4)	2.369(−1)
3–7				0–1	4.006(−1)	1.421(−1)
3–8				0–0	2.661(−4)	4.737(−2)
4–6	^{1}D–^{3}P	5.475(−2)	5.476(−2)	2–2	4.970(−2)	3.042(−2)
4–7				2–1	3.836(−3)	1.825(−2)
4–8				2–0	1.223(−3)	6.084(−3)
5–6	^{1}S–^{3}P	2.643(−3)	2.478(−3)	0–2	1.077(−3)	1.377(−3)
5–7				0–1	1.292(−2)	8.260(−4)
5–8				0–0	4.401(−4)	2.753(−4)
1–9	^{3}P–^{1}P	5.579(−3)	5.652(−3)	2–1	3.658(−2)	3.140(−2)
2–9				1–1	3.249(−3)	1.884(−3)
3–9				0–1	3.322(−3)	6.280(−4)
1–10	^{3}P–^{1}S	8.000(−5)	7.753(−5)	2–0	9.490(−5)	4.307(−5)
2–10				1–0	2.719(−5)	2.584(−5)
3–10				0–0	2.880(−5)	8.614(−6)

although still significant, importance for the $2s^22p^33l$ configurations. The present calculation, that focuses on the $2s^22p^33l$ configurations, underestimates their collisional excitation by neglecting resonances, but nevertheless it provides a dataset of reasonable accuracy for most purposes, as shown by the agreement of the intensities predicted with the present dataset and observations (see next section). Moreover, since no data are available for these configurations in the literature, our results provide an important contribution to spectral codes that otherwise would completely ignore the lines emitted by these levels. However, we strongly encourage the atomic physics community to perform extensive and accurate R-Matrix calculations of collisional excitation for Ca XIII.

5. Comparison with laboratory observations

In order to ascertain the accuracy of line emissivities calculated with the present atomic data and transition rates, we have compared them with some observations obtained from the laboratory. Most experimental works on Ca XIII report only wavelengths, but a few of them list estimates of the intensities of the observed lines (i.e. Doschek et al. 1973; Fawcett & Hayes 1975; Kaufman et al. 1982; Soukhanovskii et al. 2000). Unfortunately, Doschek et al. 1973 list only visual estimates of line intensities for transitions emitted by $2s^22p^33s$ levels, so their accuracy is limited. A comparison with our calculations shows that a few lines identified as Ca XIII correspond to very weak transitions, thus questioning the identification of the lines and pointing to the presence of a spectral feature of another ion; predicted line intensities for the remaining lines agree with measured values within a factor of two or better, with only a few exceptions. Similar problems affect the intensities published by Fawcett & Hayes (1975), who provide intensities for transitions emitted by $2s^22p^33d$ upper levels: they do not provide any indication on how their intensities were measured and whether any intensity calibration factor was taken into account. However, a comparison of predicted and measured intensities shows an encouraging agreement within a factor of two.

More detailed comparisons can be made with the measurements from Kaufman et al. (1982) and Soukhanovskii et al. (2000). Both studies measured lines from the $2s2p^5 \rightarrow 2s^22p^4$ transitions. The latter used tokamak plasma observations and provided absolutely calibrated line intensities for ^{3}P–^{3}P transitions and for the ^{1}P–^{1}D singlet. The agreement between theoretical and observed intensities is 20% or better for all

Table 7. Comparison between collision strengths from the present calculations (BL05) with the results of Baliyan & Bhatia (1994 – BB94). The incident electron energy is 120 Ry. Comparison is carried out both in intermediate and LS coupling. Baliyan & Bhatia (1994) LS coupling collision strengths have been splitted into intermediate coupling using statistical weights of levels.

Transition	LS terms	LS coupling		J values	Intermediate coupling	
		BL05	BB94		BL05	BB94
1–11	^{3}P–^{5}S	1.871(−3)	1.839(−3)	2–2	1.320(−3)	1.022(−3)
2–11				1–2	5.965(−4)	6.130(−4)
3–11				0–2	1.945(−4)	2.043(−4)
1–12	^{3}P–^{3}S	4.288(−2)	3.737(−2)	2–1	2.505(−2)	2.076(−2)
2–12				1–1	1.263(−2)	1.246(−2)
3–12				0–1	4.728(−3)	4.152(−3)
1–13	^{3}P–^{3}D	6.205(−2)	6.035(−2)	2–1	7.227(−4)	6.706(−3)
1–14				2–2	1.011(−2)	1.112(−2)
1–15				2–3	2.702(−2)	1.565(−2)
2–13				1–1	7.283(−3)	4.023(−3)
2–14				1–2	1.032(−2)	6.706(−3)
2–15				1–3	2.140(−4)	9.388(−3)
3–13				0–1	4.598(−3)	1.341(−3)
3–14				0–2	1.352(−4)	2.235(−3)
3–15				0–3	8.934(−7)	3.219(−3)
1–40	^{3}P–^{5}D	1.530(−2)	1.626(−2)	2–0	2.893(−4)	3.613(−4)
1–41				2–1	1.309(−3)	1.084(−3)
1–42				2–2	2.528(−3)	1.807(−3)
1–43				2–3	3.007(−3)	2.529(−3)
1–44				2–4	4.205(−3)	3.252(−3)
2–40				1–0	3.897(−4)	2.168(−4)
2–41				1–1	8.367(−4)	6.504(−4)
2–42				1–2	1.275(−3)	1.084(−3)
2–43				1–3	1.658(−3)	1.518(−3)
2–44				1–4	1.205(−3)	1.951(−3)
3–40				0–0	1.729(−4)	7.227(−5)
3–41				0–1	4.856(−4)	2.168(−4)
3–42				0–2	3.629(−4)	3.613(−4)
3–43				0–3	2.530(−4)	5.059(−4)
3–44				0–4	5.090(−4)	6.504(−4)

transitions but two, where the agreement is ≃40−50%. Kaufman et al. (1982) measured more transitions than Soukhanovskii et al. (2000) observing a laser-produced plasma with a grazing incidence spectrometers; they provide relative intensities although they do not mention whether they applied absolute or relative intensity calibrations. The agreement between their observations and predictions with the present data is within 40% for all of the lines, with only a few exceptions for the weakest lines in the spectrum.

We have compared the observed ratio 648.7/1133.8 between the two transitions in the ground configuration with observations from a flaring active region on the Sun observed by the SUMER instrument on SOHO. Details of the observation can be found in Feldman et al. (2000) and Landi et al. (2003). The observed region was composed by post-flare plasma at around 6–10 MK and quiescent active region plasma at 4 MK; Ca XIII lines were emitted by the latter. This ratio is density sensitive and can be used to measure the electron density N_e of the emitting plasma. We have compared its experimental value from two distinct regions in the SUMER field of view, obtaining density estimates of $\log N_e = 9.1 \pm 0.1$ and $\log N_e \leq 8.90$ (N_e in cm^{-3}), consistent with typical quiescent active region densities.

6. Diagnostic relevance of Ca XIII lines

Ca XIII line intensities can be used for a variety of diagnostic purposes, including plasma bulk motions, thermal and non-thermal Doppler motion, emission measure and differential emission measure. Since Ca XIII lines have been observed in coronal holes, quiet Sun and active regions, they can be used as diagnostic tool in a variety of different physical conditions.

Ca XIII lines can also be used for temperature and density diagnostics. Temperature sensitivity among Ca XIII lines is mostly found for transitions close in wavelength and emitted by different configurations. Such line pairs can be found in the soft X-ray range, where transitions from the 3s, 3p and 3d

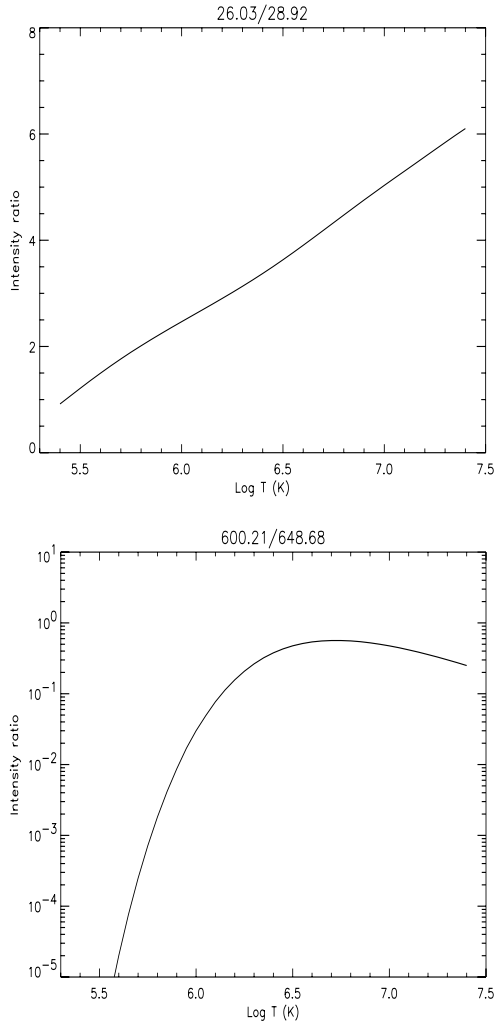

Fig. 1. Temperature diagnostics with Ca XIII lines. *Top*: using X-ray line pairs; *bottom*: using UV line pairs.

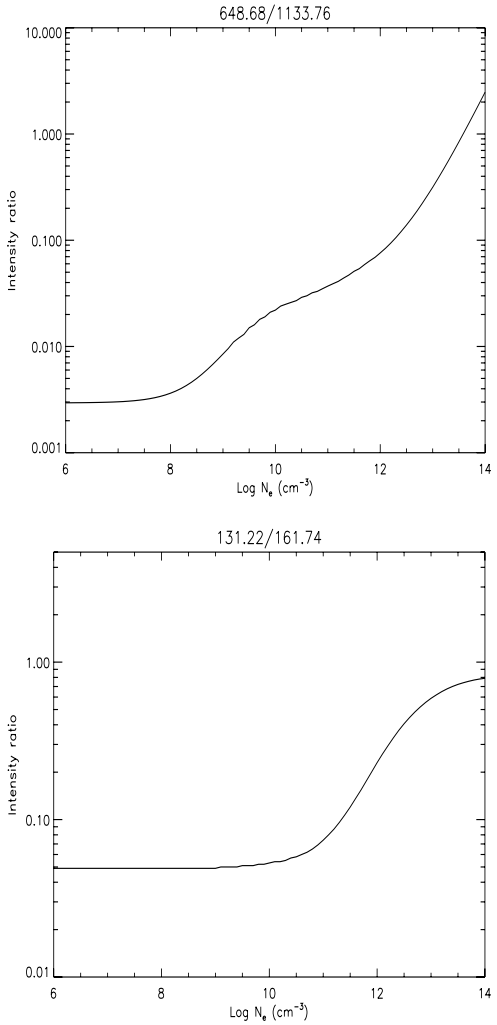

Fig. 2. Density diagnostics with Ca XIII lines. *Top*: using UV lines from the ground configuration; *bottom*: using EUV lines from allowed $n = 2$ transitions.

upper configurations can be found in a 15 Å wide wavelength interval, and in the UV range, where lines from the ground configuration and from the $n = 3$ configurations are found in close wavelength proximity. Figure 1 shows two examples of line ratios, one in the X-rays and one in the UV, that demonstrate the temperature diagnostic potential of Ca XIII.

Density sensitivity can be found in transitions within the ground configuration, and between the ground and the first excited configuration. Some density sensitivity is also present in the soft X-ray lines, but density sensitive line pairs always involve a rather weak line that is not likely to be observed. Line pairs involving two ground configuration lines in the UV range provide excellent diagnostics for densities higher than 5×10^9 cm^{-3}, as shown by the 648.7/1133 ratio displayed in Fig. 2. These densities are typical of strong active regions, where Ca XIII lines can be easily observed. Also ratios between one line from the ground configuration and one line from the $n = 3$ levels observed in the UV range can be excellent density indicators, but their temperature dependence makes their diagnostic use more difficult. The $2s^2 2p^4$–$2s2p^5$ lines in the EUV also provide density sensitive ratios when the singlet line at 131.22 Å is involved, as shown in Fig. 2.

7. Conclusions

In the present work we have carried out an ab initio calculation of atomic data and transition probabilities for the six lowest configurations of Ca XIII. We have used the distorted wave approximation to calculate collision strengths for all possible transitions between the 86 levels in the atomic model. The results compare favorably with earlier calculations, where available. The present calculation is the first one that includes collision rates for levels of the $2s^2 2p^2 3l$ (l = s, p, d) configurations, that allow the calculation of level populations and line emissivities from those configurations. Lines from these levels can be successfully used to measure the electron temperature of astrophysical and laboratory plasmas.

The present results are available on request from the authors, and they will also be incorporated in the next version of the CHIANTI database (Dere et al. 1997; Landi et al. 2005), freely distributed over the internet.

Acknowledgements. The work of Enrico Landi is supported by the NNH04AA12I, W10,232 and NNG04ED07P NASA grants.

Calculations were carried out using the Halem computer of the NASA Center for Computation Science.

References

Acton, L. W., Bruner, M. E., Brown, W. A., et al. 1985, ApJ, 291, 865
Baliyan, K. S., & Bhatia, A. K. 1993, Phys. Rev. A, 48, 250
Baliyan, K. S., & Bhatia, A. K. 1994, J. Phys. B, 27, 4281
Baluja, K. L., & Zeippen, C. J. 1988, J. Phys. B, 21, 1455
Bhatia, A. K., Landi, E., & Mason, H. E. 2003, ADNDT, 83, 71
Bromage, G. E., & Fawcett, B. C. 1977, MNRAS, 178, 591
Burgess, A., & Sheorey, V. B. 1974, J. Phys. B, 7, 2403
Burgess, A., & Tully, J. A. 1992, A&A, 254, 436
Butler, K., & Zeippen, C. J. 2001, A&A, 372, 1083
Cheng, K. T., Kim, Y. K., & Desclaux, J. P. 1979, ADNDT, 24, 111
Curdt, W., Landi, E., & Feldman, U. 2004, A&A, 427, 2004
Dere, K. P., Landi, E., Mason, H.E., Monsignori Fossi, B.C., & Young, P. R., A&AS, 125, 149
Doschek, G. A., Feldman, U., & Cohen, L. 1973, J. Opt. Soc. Am., 63, 1463
Edlen, B. 1983, Physica Scripta, 28, 51
Eissner, W. 1998, Comput. Phys. Commun., 114, 295
Eissner, W., & Seaton, M. J. 1972, J. Phys. B, 5, 2187
Eissner, W., Jones, M., & Nussbaumer, H. 1974, Comput. Phys. Commun., 8, 270
Fawcett, B. C. 1986, ADNDT, 34, 215
Fawcett, B. C., & Hayes, R. W. 1975, MNRAS, 170, 185
Feldman, U., Curdt, W., Landi, E., & Wilhelm, K. 2000, ApJ, 544, 508
Feldman, U., Landi, E., & Curdt, W. 2003, ApJ, 585, 2003
Feldman, U., Dammasch, I., Landi, E., & Doschek, G. A. 2004, ApJ, 609, 439
Froese Fischer, C., & Saha, H. P. 1983, Phys. Rev. A, 28, 3169
Gaigalas, G., Kaniauskas, J., Kisielius, R., Merkelis, G., & Vilkas, M. J. 1994, Phys. Scr., 49, 135
Galavis, M. E., Mendoza, C., & Zeippen, C. J., A&AS, 123, 159
Gu, M. F. 2003, ApJ, 582, 1241
Kaufman, V., Sugar, J., & Cooper, D. 1982, Phys. Scr., 25, 623
Jefferies, J. T., Orrall, F. Q., & Zirker, J. B. 1971, Sol. Phys., 16, 103
Landi, E., & Feldman, U. 2003, ApJ, 592, 607
Landi, E., Feldman, U., Innes, D. E., & Curdt, W. 2003, ApJ, 582, 506
Landi, E., Dere, K. P., Young, P. R., et al. 2005, ApJ, in press
Mason, H. E. 1975, MNRAS, 170, 651
Mazzotta, P., Mazzitelli, S., Colafrancesco, S., & Vittorio, N. 1998, A&AS, 133, 403
Saraph, H. E. 1978, Comput. Phys. Commun., 15, 247
Saraph, H. E., & Eissner, W. 2005, Comput. Phys. Commun., submitted
Soukhanovskii, V. A., Lippmann, S., May, M. J., et al. 2000, A&AS, 142, 95
Tachiev, G., & Froese Fischer, C., A&A, 385, 716
Vilkas, M. J., Merkelis, G., Kisielius, R., et al. 1994, Phys. Scr., 49, 592
Zhang, H. L., & Sampson, D. H. 2002, ADNDT, 82, 357